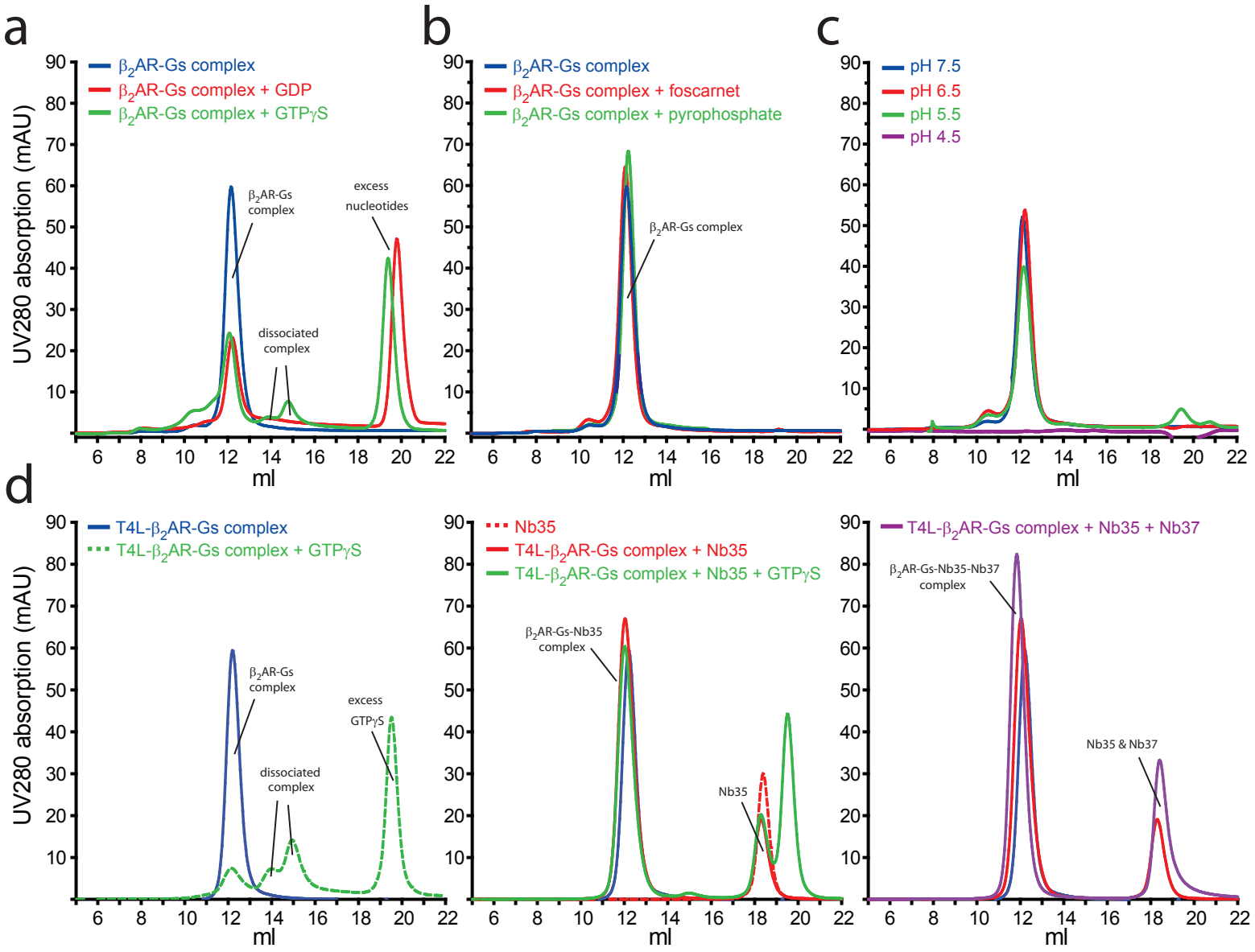

Figure S1: Effect of nucleotide analogs, pH, and nanobodies on the stability of the β_2AR-Gs complex.
a) Analytical gel filtration showing that nucleotides GDP and GTPγS (0.1 mM) cause dissociation of the β_2AR-Gs complex. b) The phosphates pyrophosphate and foscarnet (used at 5 mM) resemble the nucleotide phosphate groups, but do not cause disruption of the complex. When used as additives they improved crystal growth of both the T4L-β2AR-Gs complex (without nanobodies), T4L-β2AR-Gs-Nb37, and T4L-β2AR-Gs-Nb35. c) The pH limit was determined to guide the preparation of crystallization screens. For the same purpose the effect of ionic strength (data not shown) was determined using NaCl at various concentrations. The complex is stable in 20, 100, and 500 mM but dissociates at 2.5 M NaCl. d) Nanobody 35 (Nb35, red dashed line) binds to the β_2AR-Gs complex (blue solid line) to form the β_2AR-Gs-Nb35 complex (red solid line) which is insensitive to GTPγS treatment (green solid line) in contrast to the treated β_2AR-Gs complex alone (green dashed line). Nb35 and Nb37 binds separate epitopes on the Gs heterotrimer to form a β_2AR-Gs-Nb35-Nb37 complex (purple solid line). Nb37 binding also prevents GTPγS from dissociating the β_2AR-Gs complex (data not shown).

Figure S2: Crystals of the T4L-β_2AR-Gs-Nb35 complex in sponge-like mesophase

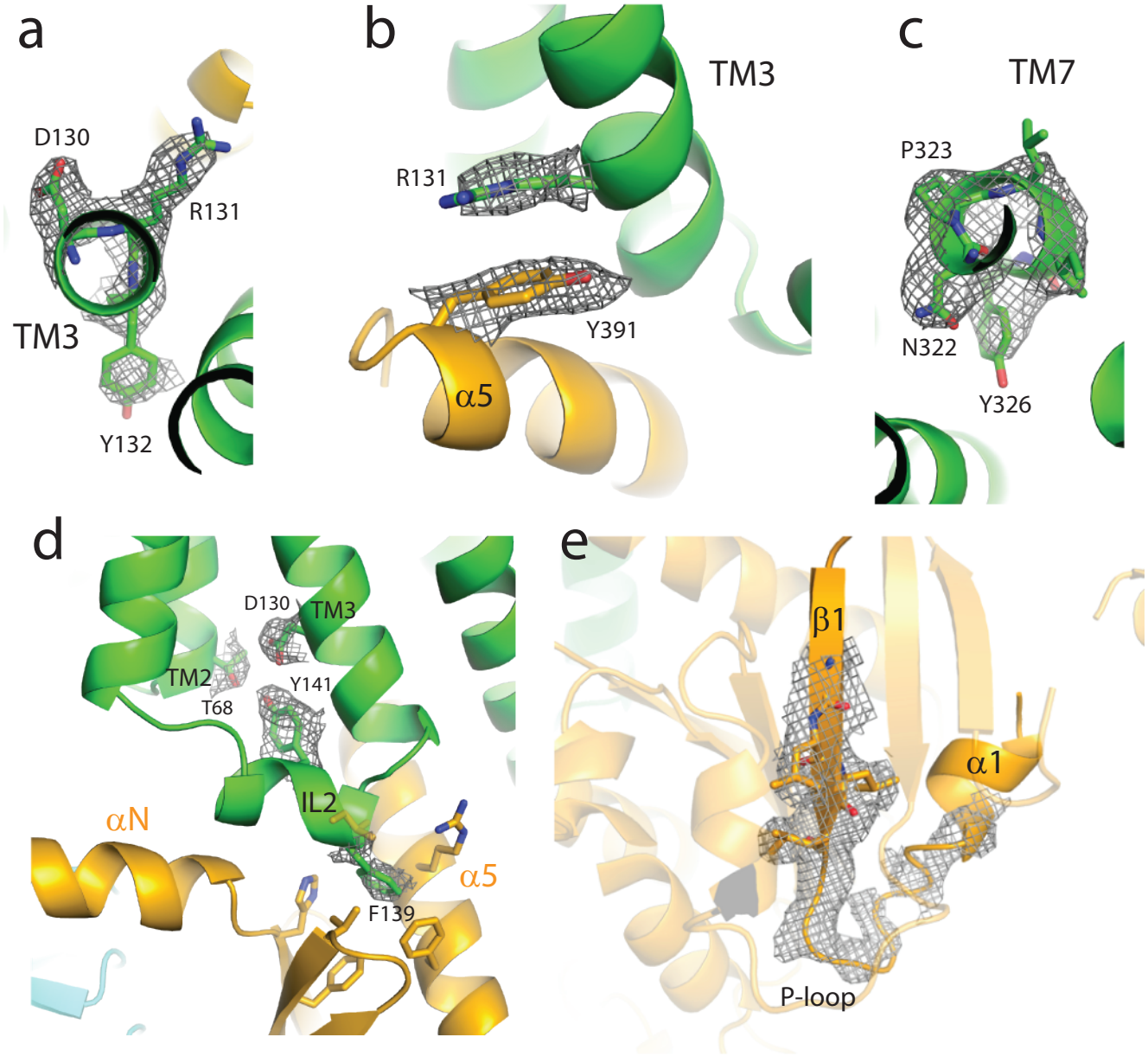

Figure S3: Views of electron density for residues in the β_2AR-Gs interface.
a) The D/ERY motif at the cytoplasmic end of TM3. b) Packing interaction between Arg131 of the E/DRY motif and Tyr391 of C-terminal Gαs. c) The NPxxY in the cytoplasmic end of TM7. d) Interactions of Thr68 and Tyr141 with Asp130 of the E/DRY motif. Phe139 of IL2 is buried in a hydrophobic pocket in Gαs. e) The β1-α1 loop (P-loop) of Gαs involved in nucleotide binding.

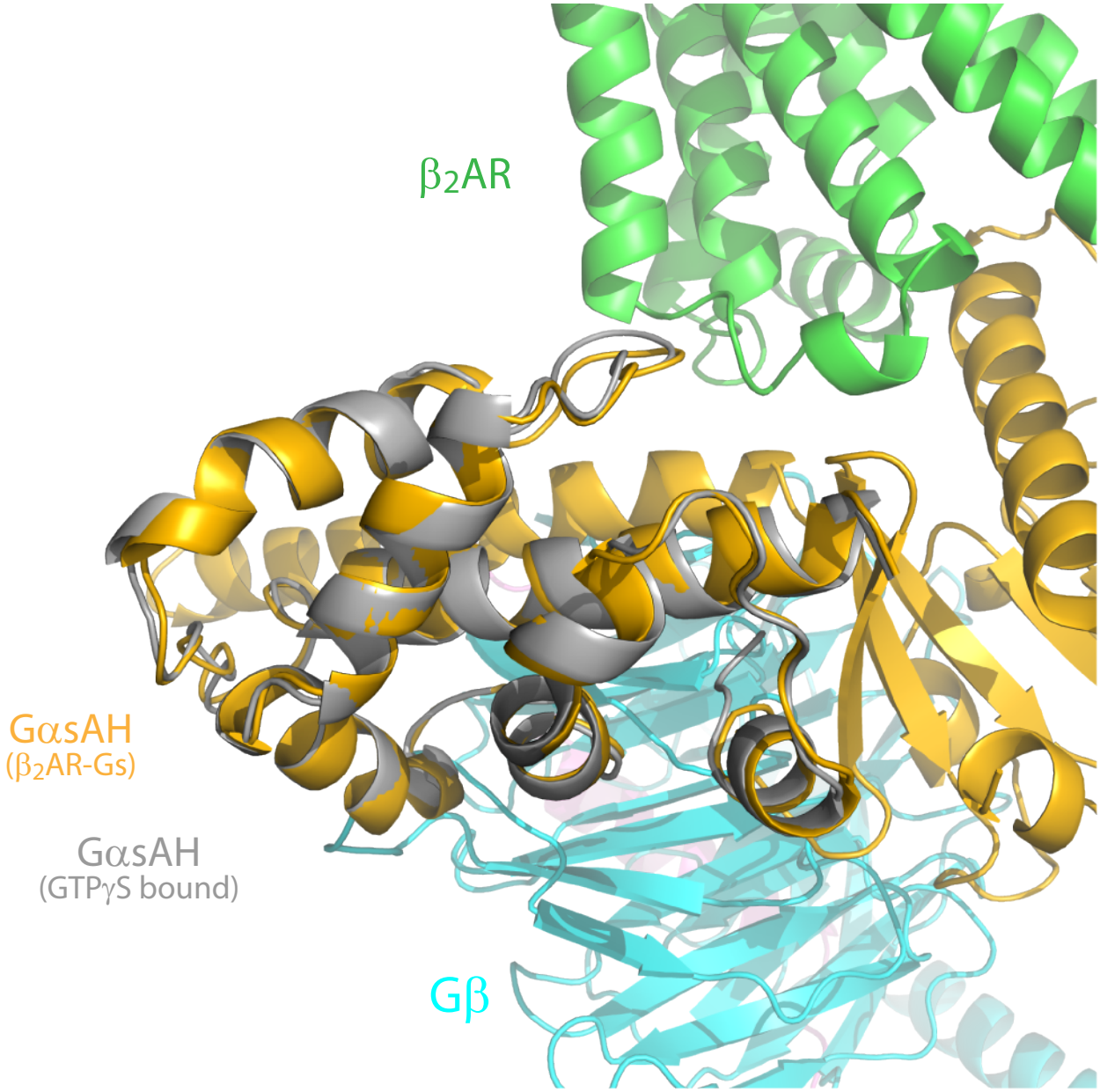

Figure S4: Rigid body motion of the alpha helical domain
The GαsAH domain of the GTPγS bound structure (1AZT, Sunahara et al.) was aligned with GαsAH domain of the nucleotide-free β_2AR-Gs structure to show that the displacement of GαsAH is a rigid body movement without significant intradomain conformational changes.

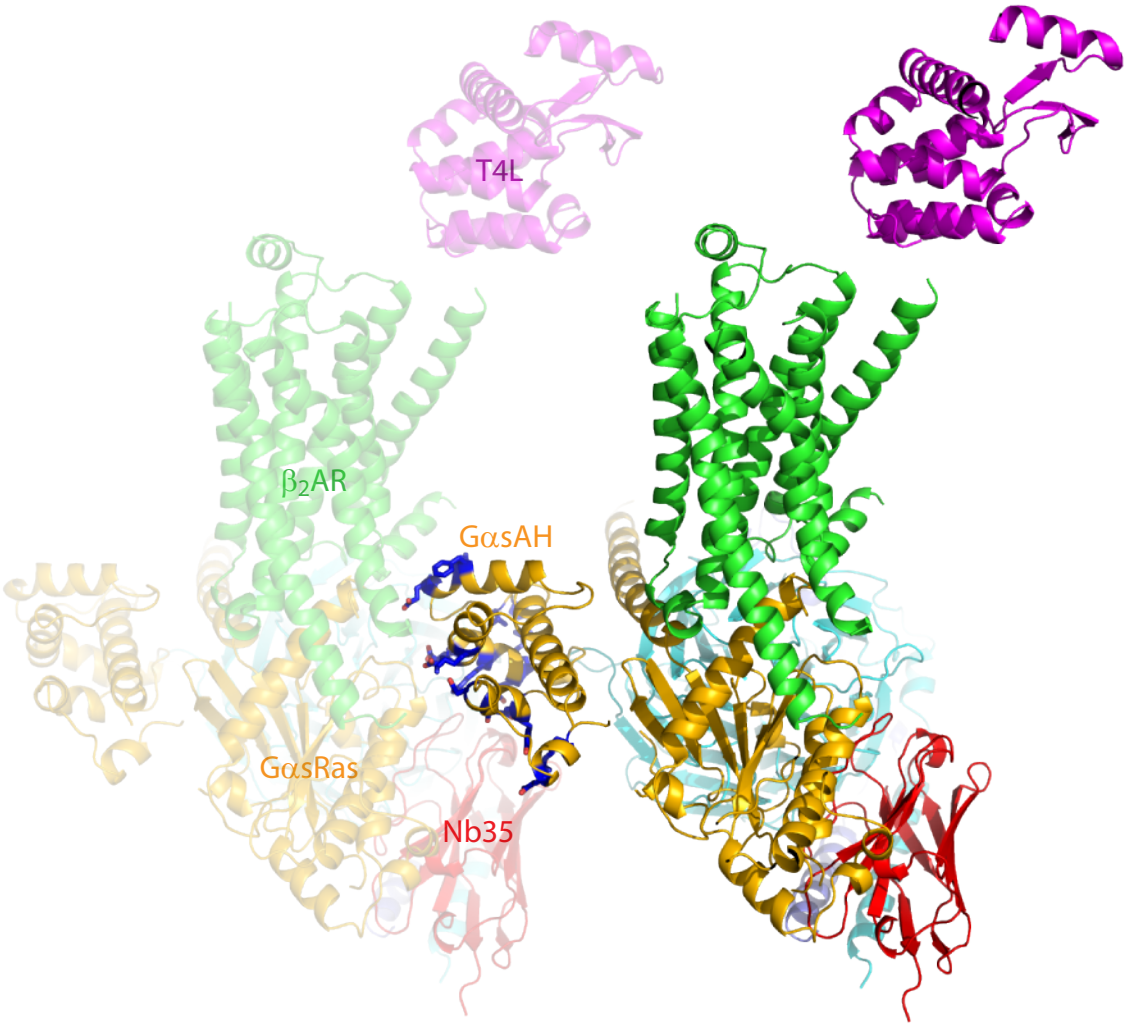

Figure S5: Packing interactions of GαsAH domain
Shown in blue are residues in the GαsAH domain that are within 5Å of neighboring lattice contacts on Nb35, the GαsRas domain, and the β_2AR.

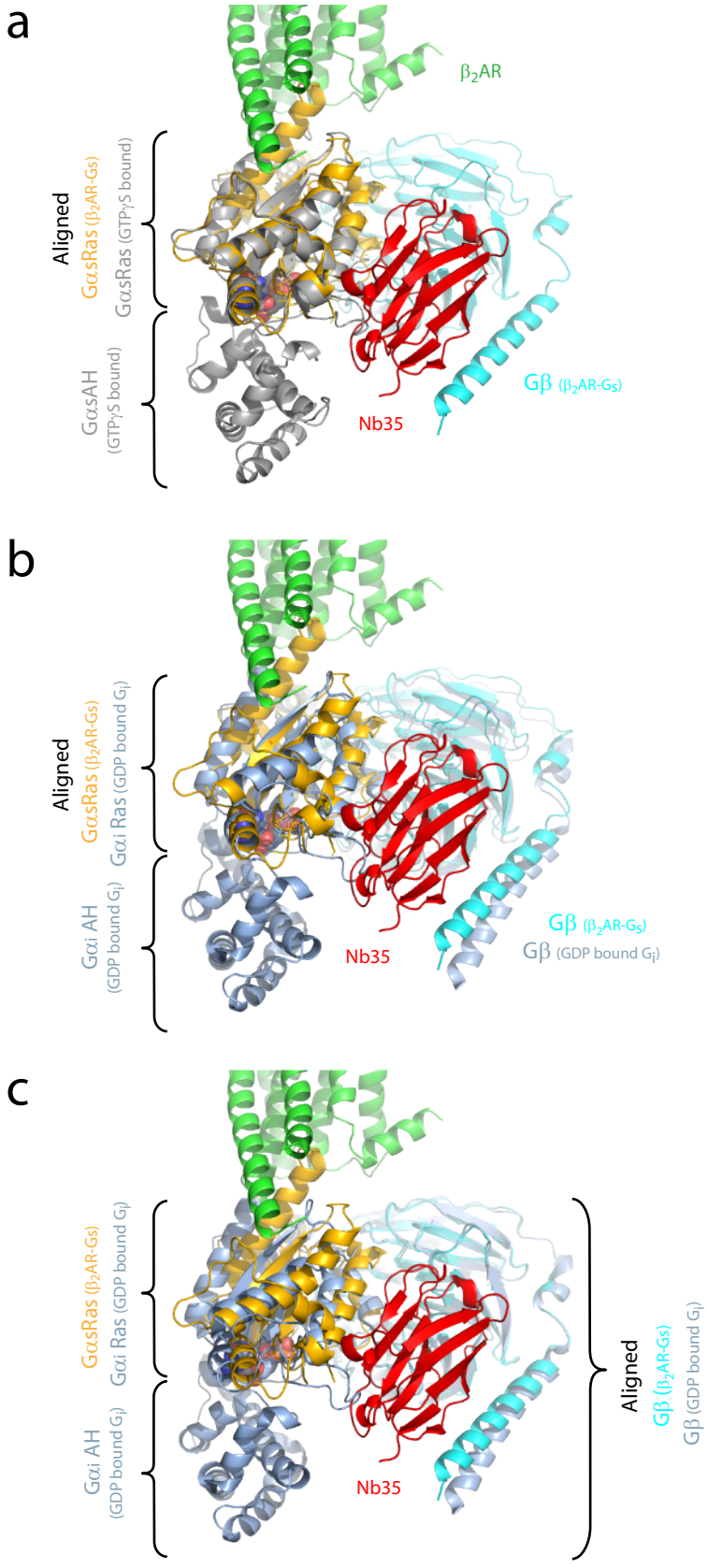

Figure S6: Displacement of GαsAH domain is not caused by a steric clash with Nb35
The GαsRas domain of the β_2AR-G_s structure was aligned with the GαsRas domain of the GTPγS bound structure (1AZT, Sunahara et al.) in (a) and with GαiRas domain of GDP bound G_i structure (1GP2, Wall et al.) in (b). c) The Gβ of the β_2AR-G_s structure was aligned with Gβ of the GDP bound G_i structure. In all three alignments, Nb35 (in red) does not overlap with the space occupied by the nucleotide bound state of the alpha helical domain in the Gαs-GTPγS and G_i-GDP structures.

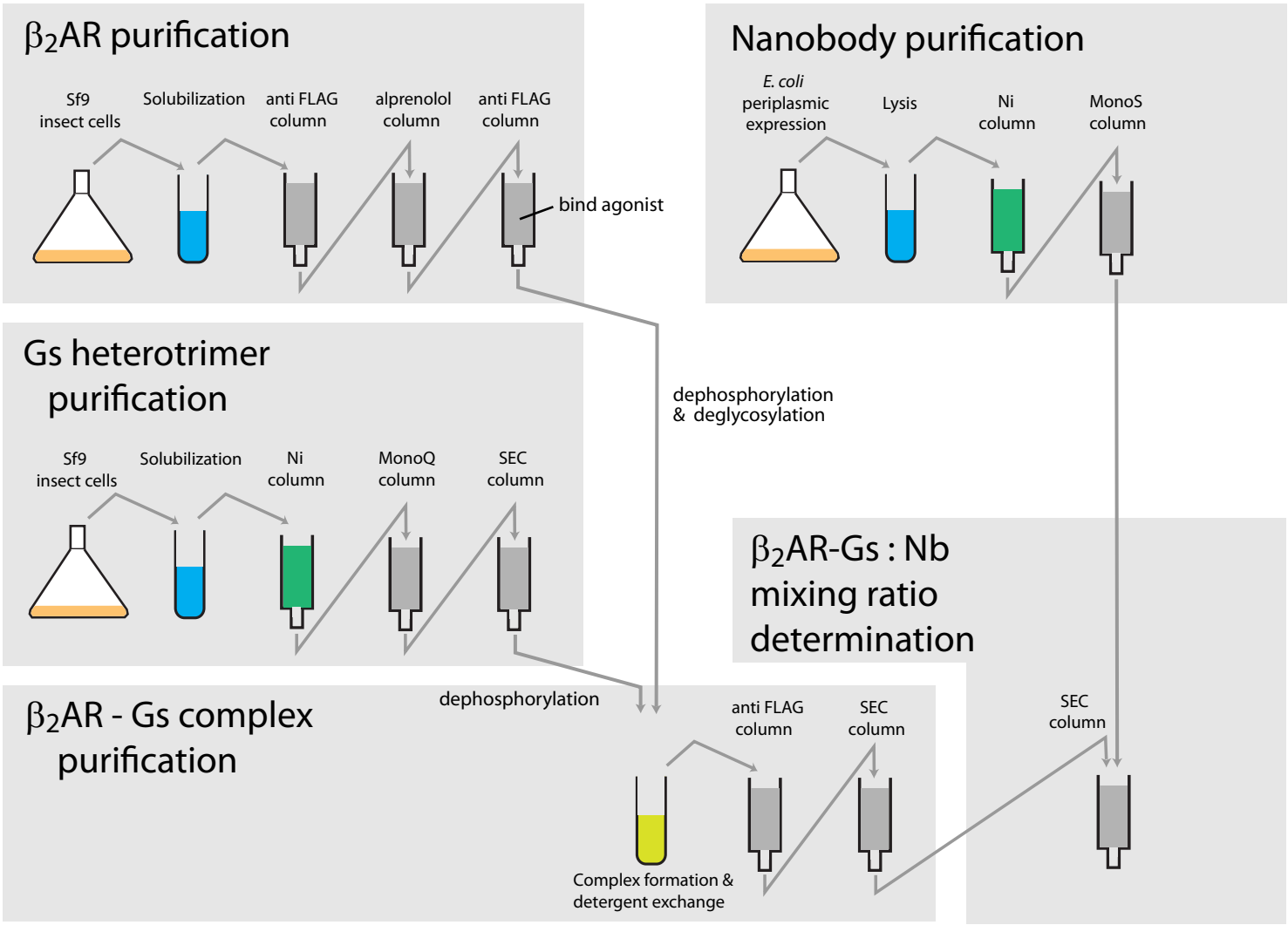

Figure S7: Flow-chart of the purification procedures for preparing β_2AR-Gs complex with Nb35

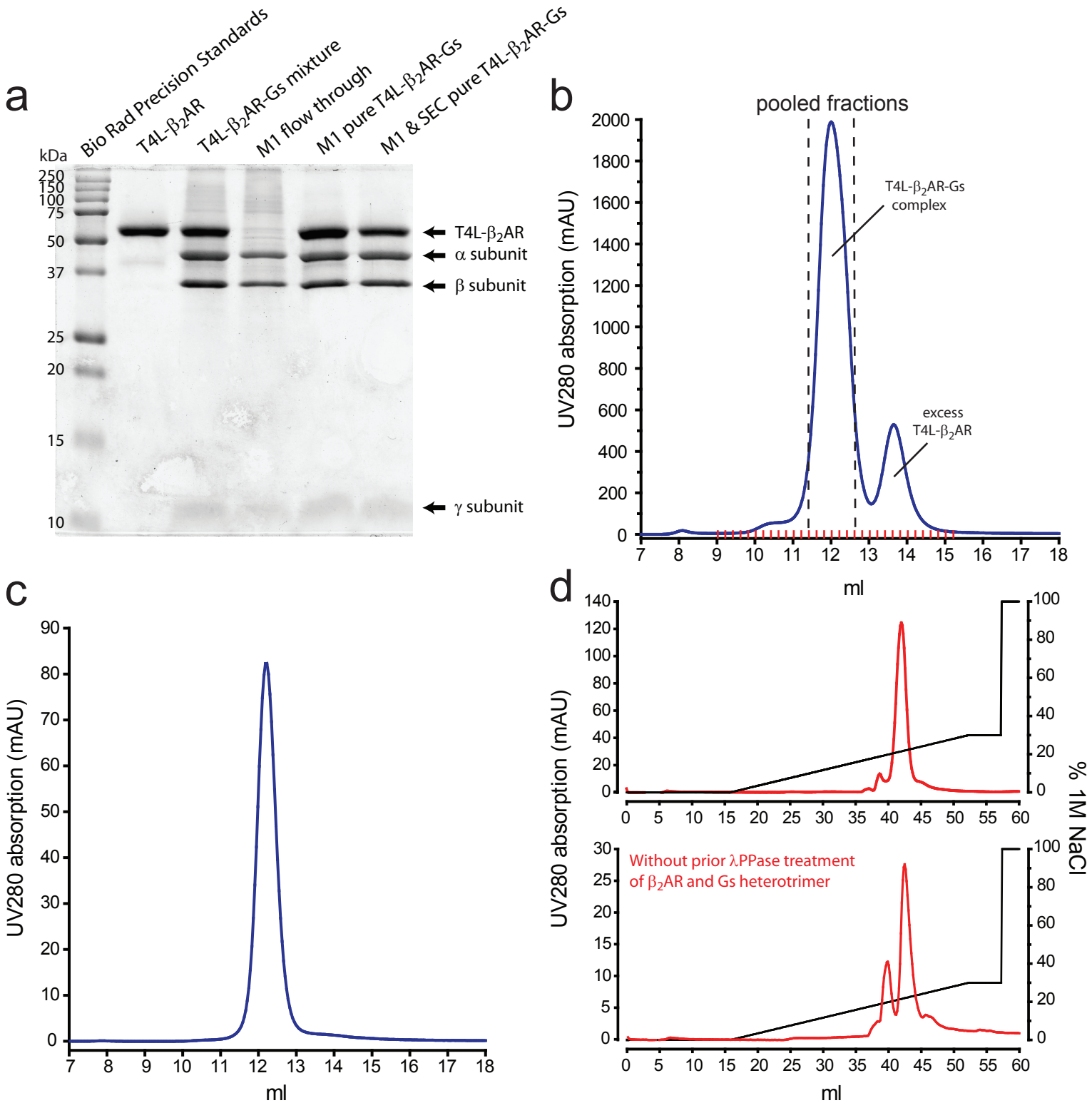

Figure S8: Purity and homogeneity of the β_2AR-Gs complex

a) Analytical SDS-PAGE/Coomassie blue stain of samples obtained at various stages of β_2AR-Gs purification. BI-167107 agonist bound, dephosphorylated, and deglycosylated receptor is used in excess of Gs heterotrimer for optimal coupling efficiency with the functional fraction of the G protein. Functional purification of Gs is achieved through its interaction with the immobilized receptor on M1 resin while non-functional/non-binding Gs is not retained. b) A representative elution profile of one of four consecutive preparative size exclusion chromatography (SEC) runs with fractionation indicated in red. SEC fractions containing the β_2AR-Gs complex (within the indicated dashed lines) were pooled, spin concentrated, and analyzed for purity and homogeneity by SDS-PAGE/Coomassie blue (a, lane 6), gel filtration (c), and by anion exchange chromotography (d). d) Upper panel shows elution profile from an analytical ion exchange chromatography (IEC) run of β_2AR-365-Gs complex that was treated with λ phosphatase prior to complex formation. Lower panel shows IEC of complex which was not dephosphorylated resulting in a heterogeneous preparation. Off-peak fractions from the preparative SEC (b) were used for analytical gel filtration experiments shown in figures S1 and S12.

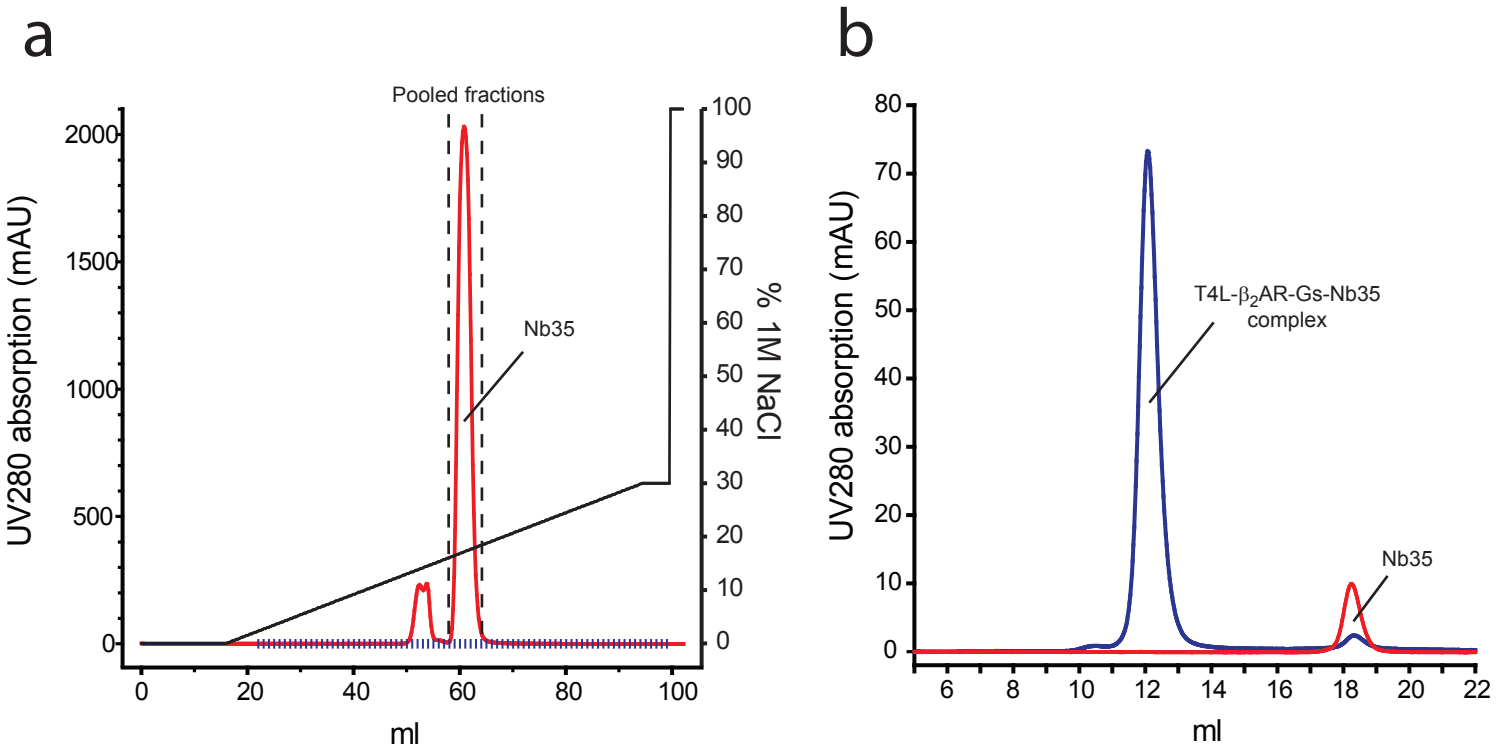

Figure S9: Purification of Nb35 and determination of β_2AR:Gs:Nb mixing ratio

a) Preparative ion exchange chromotography following nickel affinity chromotography purification of Nb35. The nanobody eluted in two populations (shown in red) as a minor peak and a major homogeneous peak which was collected, spin concentrated, and used for crystallography following determination of proper mixing ratio with the β_2AR-Gs complex as shown in (b). b) The β_2AR-Gs complex was mixed with slight excess of Nb35 (1 to 1.2 molar ratio of β_2AR-Gs complex to Nb35) on the basis of their protein concentrations and verified by analytical gel filtration.

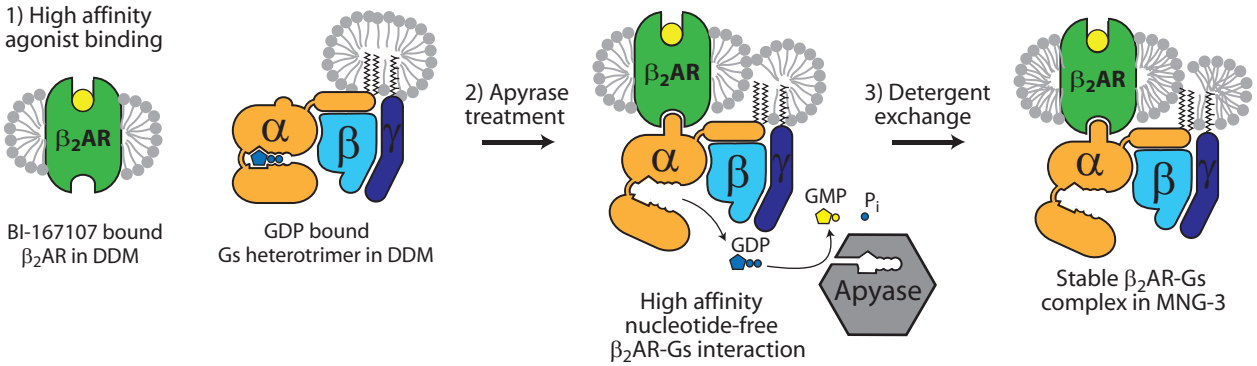

Figure S10: Formation of a stable β_2AR-Gs complex.

A stable complex was achieved by the combined effects of: 1) binding a high affinity agonist to the receptor with an extremely slow dissociation rate (as described in Rasmussen et al., 2011); 2) formation of a nucleotide free complex in the presence of apyrase, which hydrolyses released GDP preventing it from rebinding and causing dissociation of the β_2AR-Gs complex; and 3) detergent exchange of DDM for MNG-3 which stabilizes the complex.

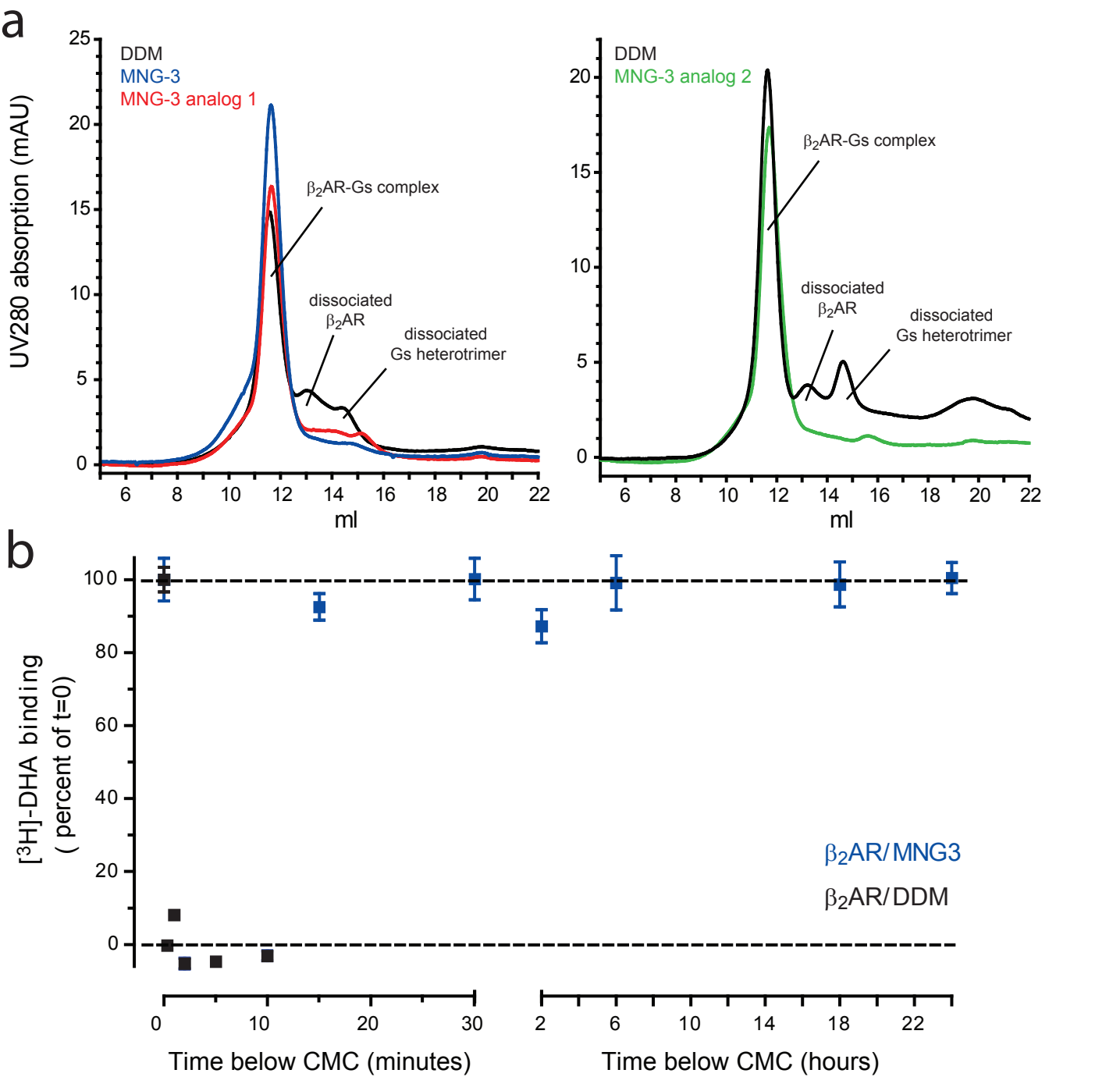

Figure S11: Stabilizing effect of MNG-3 on the β_2AR-Gs complex

a) Analytical gel filtration of β_2AR-Gs complexes purified in DDM (in black), MNG-3 (in blue), or two MNG-3 analogs (in red and green) following incubation for 48 hrs at 4°C . In contrast to DDM, the β_2AR-Gs complexes are stable in the MNG detergents. b) Effect of diluting unliganded purified β_2AR in either DDM or MNG-3 below the critical micelle concentration (CMC) of the detergent. Functional activity of the receptor was determined by [^{3}H]-dihydro alprenolol ([^{3}H]-DHA) saturation binding. Diluting β_2AR maintained in DDM by 1000-fold below the CMC causes loss of [^{3}H]-DHA binding (black data points) after 20 sec. In contrast, β_2AR in MNG-3 diluted 1000-fold below the CMC maintained full ability to bind [^{3}H]-DHA after 24 hrs.

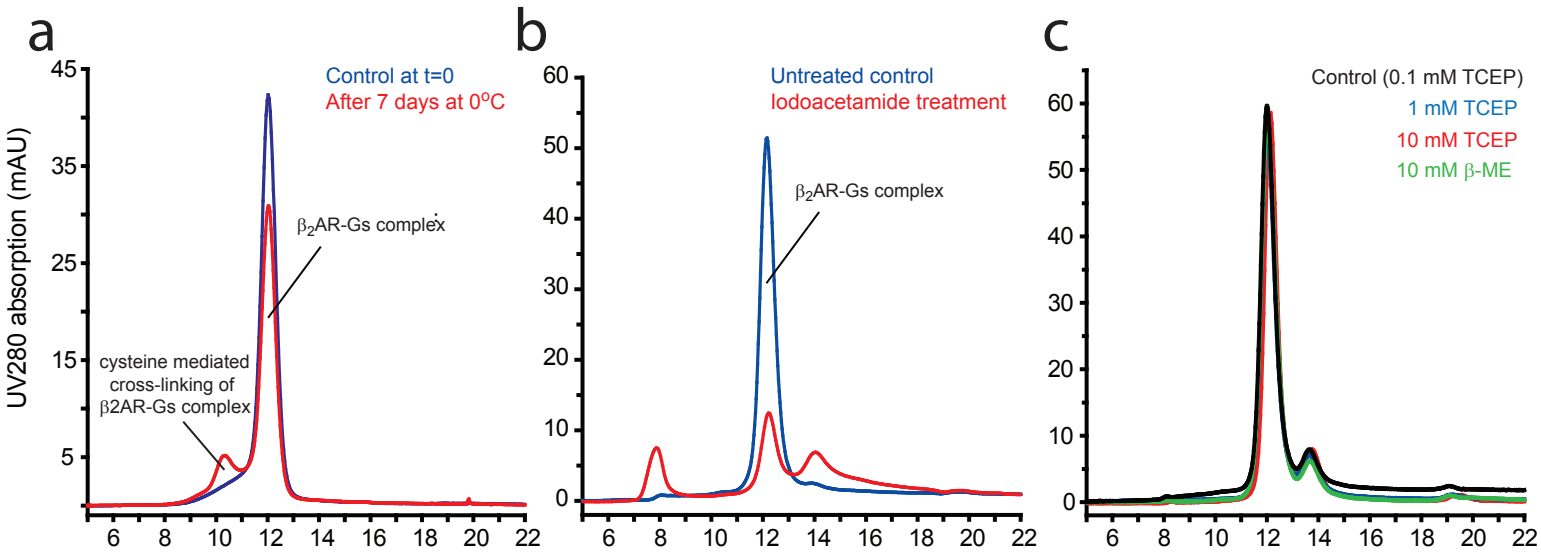

Figure S12: Effect of alkylating and reducing agents on the stability and aggregation of the β_2AR-Gs complex.
a) Disulfide-mediated aggregation of the β_2AR-Gs complex was observed by size exclusion chromatography (SEC) following incubation at 0° C for 7 days in buffer containing 0.1 mM tris(2-carboxyethyl)phosphine (TCEP). b) Treatment of the complex with iodoacetamide (5 mM for 20 hrs at 20° C) led to dissociation of the complex. Alkylating free cysteines with iodoacetic acid and cadmium chloride also led to dissociation. c) Disulfide-mediated aggregation of the complex could be prevented by higher concentrations of reducing agents. Treatment of the β_2AR-Gs complex with 0.1, 1, and 10 mM TCEP for 1 hr at 20° C, or 10 mM betamercaptoethanol (β-ME, 1 hr at 20° C) did not lead to dissociation or aggregation. Crystallization setups were performed using 1 to 5 mM TCEP, which was essential for optimal crystal growth.

Supplementary Table 1: Potential intermolecular interactions within the β_2AR-Gs interface

	atom in β_2AR	atom in Gαs		distance (Å)
TM3	[ARG 131 CG]	[TYR 391 CE2]	α5	3.6
	[ALA 134 O]	[HIS 387 ND1]	α5	3.1
	[ALA 134 CB]	[HIS 387 ND1]	α5	3.8
	[ALA 134 CB]	[HIS 387 CG]	α5	3.8
	[ILE 135 O]	[GLN 384 NE2]	α5	2.9
	[ILE 135 CD1]	[LEU 388 CD1]	α5	3.5
	[ILE 135 CD1]	[LEU 393 CD1]	α5	3.5
	[THR 136 O]	[ARG 380 NH2]	α5	3.0
IL2	[PRO 138 O]	[ILE 383 CD1]	α5	3.4
	[PRO 138 CG]	[GLN 384 CG]	α5	3.3
	[PHE 139 CD2]	[HIS 41 NE2]	– β1	3.6
	[PHE 139 CB]	[VAL 217 CG2]	– α4	3.7
	[PHE 139 CE1]	[PHE 376 CZ]	α5	3.3
	[PHE 139 CZ]	[CYS 379 C]	α5	3.9
	[PHE 139 CZ]	[ARG 380 N]	α5	3.2
	[TYR 141 CD2]	[HIS 387 NE2]	α5	3.9
	[GLN 142 OE1]	[HIS 387 NE2]	α5	3.5
	[SER 143 OG]	[ALA 39 CB]	– αN	3.6
TM5	[VAL 222 CG1]	[LEU 393 CD1]	α5	3.7
	[GLU 225 OE2]	[GLN 384 NE2]	α5	3.0
	[ALA 226 CA]	[LEU 388 CD2]	α5	3.6
	[ALA 226 CB]	[LEU 393 O]	α5	3.8
	[GLN 229 NE2]	[ASP 381 OD1]	α5	3.6
	[GLN 229 NE2]	[GLN 384 OE1]	α5	2.8
	[GLN 229 OE1]	[ARG 385 NE]	α5	3.4
	[GLN 229 CG]	[LEU 388 CD2]	α5	3.9
	[LEU 230 CG]	[LEU 394 CD1]	α5	3.5
	[LYS 232 NZ]	[ASP 381 OD1]	α5	3.1
	[ILE 233 CD1]	[TYR 358 OH]	– β6	3.4
	[ILE 233 CG1]	[ARG 385 NH1]	– α5	3.5
	[ARG 239 NE]	[THR 350 OG1]	– α4	3.5
TM6	[ALA 271 CB]	[LEU 393 O]	α5	3.0
	[THR 274 CG2]	[GLU 392 O]	α5	3.4
	[THR 274 OG1]	[LEU 393 CD2]	α5	3.3
	[LEU 275 CD2]	[LEU 393 CD2]	α5	3.6

Supplementary Table 2: Data collection and refinement statistics

Data collection*	
Number of crystals	20
Space group	P 2_1
Cell dimensions	
a, *b*, *c* (Å)	119.3, 64.6, 131.2
α, β, γ (°)	90.0, 91.7, 90.0
Resolution (Å)	41 – 3.2 (3.26 – 3.20)
R_{merge} (%)	15.6 (55.3)
$\langle I \rangle / \langle \sigma I \rangle$	10.8 (1.8)
Completeness (%)	91.2 (53.9)
Redundancy	6.5 (5.0)
Refinement	
Resolution (Å)	41 – 3.2
No. reflections	31075 (1557 in test set)
R_{work}/R_{free} (%)	22.6 / 27.8
No. atoms	10275
No. protein residues	1318
Anisotropic *B* tensor	B_{11}= -6.4 / B_{22}= 3.8 / B_{33}= 2.6 / B_{13}= 1.9
Unmodelled sequences[a]	
β_2 adrenergic receptor	29[b], 176-178, 240-264, 342-365
G_s α	1-8, 60-88, 203-204, 256-262
G_s γ	1-4, 63-68
T4 lysozyme	161[c]
Average *B*-factors (Å^2)	
β_2 adrenergic receptor	131.6
G_s α, ras domain	81.4
G_s α, helical domain	121.9
G_s β	63.0
G_s γ	83.6
Nanobody 35	59.5
T4 lysozyme	112.1
R.m.s. deviation from ideality	
Bond length (Å)	0.007
Bond angles (°)	0.71
Ramachandran statistics[d]	
Favored regions (%)	95.4
Allowed regions (%)	4.6
Outliers (%)	0

* Highest shell statistics are in parentheses. [a]These regions were omitted from the model due to poorly resolved electron density. Unmodeled purification tags are not

included in these residue ranges. [b]Residues 1-28 of the β_2AR were omitted from the construct and T4L was fused to the amino terminus of transmembrane helix 1 to facilitate crystallization. [c]Residue 1 of T4L was omitted from the construct [d]As defined by MolProbity[38].

Supplementary Table 3: Data collection statistics by resolution shell

Resolution Shell (Å)	**$\langle I \rangle / \langle \sigma I \rangle$**	**R_{merge} (%)**	**Completeness (%)**
41 - 8.67	18.8	06.6	97.1
8.67 - 6.89	16.9	09.2	99.5
6.89 - 6.02	14.4	13.0	99.7
6.02 - 5.47	12.8	16.7	99.9
5.47 - 5.08	13.4	15.9	99.9
5.08 - 4.78	13.4	16.9	99.8
4.78 - 4.54	12.2	18.2	99.6
4.54 - 4.34	11.6	20.1	99.8
4.34 - 4.18	9.5	22.9	99.4
4.18 - 4.03	7.7	26.2	99.1
4.03 - 3.91	6.6	27.9	98.7
3.91 - 3.79	5.3	30.2	98.7
3.79 - 3.69	3.8	36.6	96.7
3.69 - 3.60	4.6	36.9	94.6
3.60 - 3.52	2.3	45.7	90.3
3.52 - 3.45	2.2	47.9	86.3
3.45 - 3.38	2.4	45.6	80.5
3.38 - 3.31	2.1	47.3	69
3.31 - 3.26	2.2	49.8	59.4
3.26 - 3.20	1.8	55.3	53.9
Overall	**10.8**	**15.6**	**91.2**